DOI: 10.1002/ejic.201001215

Spin-Canted Antiferromagnetic Phase Transitions in Alternating Phenoxo- and Carboxylato-Bridged Mn^{III}-Salen Complexes

Paramita Kar,[a] Pampa M. Guha,[a] Michael G. B. Drew,[b] Takayuki Ishida,*[c] and Ashutosh Ghosh*[a]

Keywords: Manganese complexes / Salen / Magnetic properties / Spin canting

Three new Mn^{III} complexes, $\{[Mn_2(salen)_2(OCn)](ClO_4)\}_n$ (**1**), $\{[Mn_2(salen)_2(OPh)](ClO_4)\}_n$ (**2**) and $\{[Mn_2(salen)_2(OBz)](ClO_4)\}_2$ (**3**) (where salen = *N*,*N*′-bis(salicylidene)-1,2-diaminoethane dianion, OCn = cinnamate, OPh = phenylacetate and OBz = benzoate), have been synthesized and characterized structurally and magnetically. The crystal structures reveal that all three structures contain *syn-anti* carboxylate-bridged dimeric $[Mn_2(salen)_2(OOCR)]^+$ cations (OOCR = bridging carboxylate) that are joined together by weak Mn···O(phenoxo) interactions to form infinite alternating chain structures in **1** and **2**, but the relatively long Mn···O(phenoxo) distance [3.621(2) Å] in **3** restricts this structure to tetranuclear units. Magnetic studies showed that **1** and **2** exhibited magnetic long-range order at T_N = 4.0 and 4.6 K (T_N = Néel transition temperature), respectively, to give spin-canted antiferromagnetic structures. Antiferromagnetic coupling was also observed in **3** but no peaks were recorded in the field-cooled magnetization (FCM) or zero-field-cooled magnetization (ZFCM) data, indicating that **3** remained paramagnetic down to 2 K. This dominant antiferromagnetic coupling is attributed to the carboxylate bridges. The ferromagnetic coupling expected due to the Mn–O(phenoxo)···Mn bridge plays an auxiliary role in the magnetic chain, but is an essential component of the bulk magnetic properties of the material.

Introduction

In recent years considerable attention has been focused on the design and synthesis of molecular magnetic materials to further our understanding of fundamental magnetic interactions and magneto-structural correlations, as well as for the development of new molecule-based materials.[1] Magnetic phase transitions in molecular materials are of interest from a fundamental point of view, with regards to investigating novel magnetic behaviors that differ from those of traditional magnets based on metal or ionic lattices, but also with an aim of eventually synthesizing new magnetic materials.

Binuclear phenoxo-bridged manganese(III) compounds containing salen-type Schiff bases are well established, and are of interest to chemists because of their important roles in biological systems e.g. in many metalloenzymes, redox and nonredox proteins,[2,3] and as catalysts in olefin epoxidation reactions.[4] However, recent interest in this type of compound has increased since Miyasaka et al.[5] reported a dimeric manganese(III) Schiff base compound, $[Mn_2(saltmen)_2(ReO_4)_2]$ [H_2saltmen = *N*,*N*′-(1,1,2,2-tetramethylethylene)bis(salicylideneimine)] showing single-molecule magnet (SMM) behavior. Studies of these complexes show that such compounds can be both ferromagnetic and antiferromagnetic, and modulation of the Mn^{III}···Mn^{III} magnetic interaction is possible by varying the apical ligands and the chemical features of the Schiff-base ligand.[6] On the other hand, carboxylate bridging ligands displaying multiple bridging modes are able to mediate effectively magnetic coupling between metal ions, and have often been used to prepare molecular magnetic materials.[7] The versatility of carboxylates as ligands is illustrated by the variety of their coordination modes when acting as a bridge,[8–11] the most common being the so-called *syn-syn*, *syn-anti*, and *anti-anti* modes. Numerous magnetic materials exhibiting diverse bulk magnetic behavior such as antiferromagnetism, ferromagnetism, spin crossover, spin canting, and ferrimagnetism have been constructed by exploiting the different coordination modes and structural features of carboxylates.[12–15] Considering these facts, it may be expected that a system containing both phenoxo- and carboxylate-bridged Mn^{III} ions would show interesting magnetic behavior.

Herein, we report the synthesis, XRD determined single crystal structure, and magnetic properties of three new Mn^{III} Schiff-base complexes consisting of the dinuclear

[a] Department of Chemistry, University College of Science, University of Calcutta,
92, A.P.C. Road, Kolkata 700009, India
E-mail: ghosh_59@yahoo.com
[b] School of Chemistry, The University of Reading,
P. O. Box 224, Whiteknights, Reading RG 66AD, UK
[c] Department of Engineering Science, The University of Electro-Communications,
Chofu, Tokyo 182-8585, Japan
E-mail: ishi@pc.uec.ac.jp

Supporting information for this article is available on the WWW under http://dx.doi.org/10.1002/ejic.201001215.

units $[Mn_2(salen)_2(OOCR)](ClO_4)$, where R = C_6H_5-CH=CH- (**1**), $C_6H_5CH_2$- (**2**) and C_6H_5- (**3**). In complexes **1** and **2** the dinuclear cationic units are joined together by weak Mn···O (phenoxo) interactions to form an alternating phenoxo- and carboxylato-bridged 1D chain. Complex **3** is best considered to be a tetramer that is formed by the phenoxo bridge between two dimers. Interestingly, complexes **1** and **2** show antiferromagnetic phase transitions that can be explained on the basis of spin canting, whereas complex **3** behaves as a paramagnet with appreciable antiferromagnetic coupling. Long-range ordering was found to be present in **1** and **2** due to the existence of interchain magnetic interactions. To the best of our knowledge, this is the first report of the magnetic behavior of such alternating phenoxo-carboxylato-bridged Mn^{III} Schiff-base complexes.

Results and Discussion

Syntheses

Compounds **1**–**3** were obtained as dark brown micro crystals by slow evaporation of methanol solutions of $Mn(ClO_4)_2·6H_2O$, H_2salen, the corresponding carboxylic acid and triethylamine in 2:2:1:1 ratios. The Mn^{II} ions were oxidized to Mn^{III} by the oxygen in the atmosphere under these reaction conditions, and the deprotonated Schiff-base ligand (salen) molecules occupy the equatorial planes of the Mn^{III} sites, as is usual for salen-type Schiff-base complexes. Such a $[Mn(salen)]^+$ species can take up neutral or anionic ligands in one or both axial positions resulting in various complexes. In the present investigation, we maintained the molar ratios of Mn^{II} and carboxylate as 2:1, so that a carboxylate ions will bridge two manganese(III)-salen species by coordinating at one of the axial positions while keeping the other axial site vacant and thus available for interaction with phenoxo oxygen atoms of neighboring dinuclear units to generate polymeric structures (Scheme 1). Maintaining the ratio of Mn^{II} and carboxylate as 2:1 is important because a higher proportion of $Mn(ClO_4)_2·6H_2O$ in the reaction mixture led to the formation of $[Mn(salen)(H_2O)]ClO_4$ as an impurity in all three cases; on the other hand, a higher proportion of carboxylic acid resulted in the formation of another species, which was shown by elemental analysis to have the probable molecular formula of [Mn(salen)-(RCOO)(H_2O)], along with the desired complexes **1**–**3**.

Description of the Structures

All three structures contain $[Mn_2(salen)_2(OOCR)]^+$ cations (OOCR = bridging carboxylate) together with a discrete perchlorate anion in the asymmetric unit. In all three structures, the dimeric cations are involved in weak interactions with adjacent molecules to form polymeric chains in **1** and **2** and tetramers in **3**; however the perchlorate anions are not involved in any close interactions with the metal atoms.

$\{[Mn_2(salen)_2(OCn)](ClO_4)\}_n$ (1). The asymmetric unit of **1** consists of a dimeric structure that is shown in Figure 1 together with the atomic numbering scheme for the metal coordination spheres. Selected bond lengths and angles are summarized in Table 1. Within the asymmetric unit, both metal ions can be considered as five-coordinate, with square pyramidal (4 + 1) coordination spheres, when one takes into account only the five strong bonds in which the metal ions participate. However, both manganese ions are weakly co-

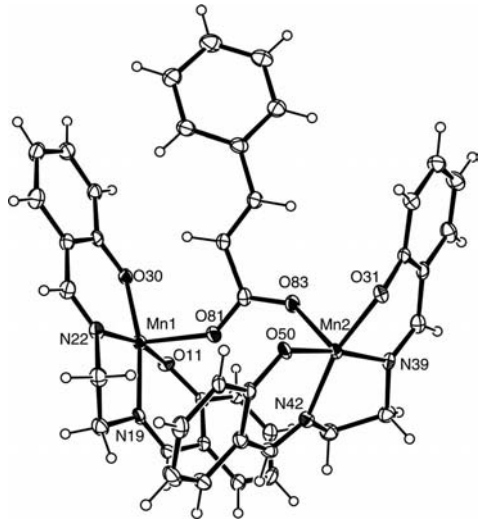

Figure 1. The dimeric structure of **1** with ellipsoids drawn at the 30% probability level.

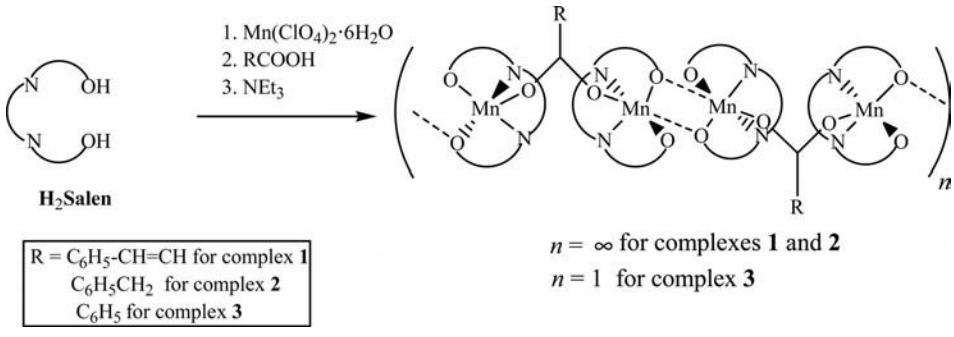

Scheme 1. Formation of complexes **1**–**3**.

ordinated at their second axial positions, which make their effective coordination number six with tetragonal coordination geometry and allow the formation of polymeric 1-D chains. The two metal ions Mn(1) and Mn(2) are coordinated by the four donor atoms of the deprotonated tetradentate Schiff-base ligand (salen) at the equatorial sites. The bond lengths are as expected with Mn–O(ligand) length within the range 1.871(2)–1.879(2) Å, and with Mn–N lengths within the 1.966(3)–1.982(3) Å range. The two oxygen atoms O(81) and O(83) of the cinnamate ligand coordinate at the axial positions of Mn(1) and Mn(2), with corresponding bond distances of 2.075(2) and 2.137(3) Å, respectively, to form a *syn-anti* carboxylate bridge between the two Mn ions. These axial bonds are significantly longer than the equatorial bonds, which is a result of Jahn–Teller distortion due to the Mn ions being in the +3 oxidation state.

Table 1. Bond lengths [Å] and angles [°] in the metal coordination spheres of complex **1**–**3**.

	1	**2**	**3**
Mn(1)–O(11)	1.871(2)	1.856(4)	1.865(2)
Mn(1)–O(30)	1.899(2)	1.907(4)	1.908(2)
Mn(1)–N(19)	1.966(3)	1.977(5)	1.971(2)
Mn(1)–N(22)	1.997(3)	1.975(4)	1.993(2)
Mn(1)–O(81)	2.075(2)	2.110(4)	2.098(2)
Mn(2)–O(31)	1.875(2)	1.867(4)	1.874(2)
Mn(2)–O(50)	1.879(2)	1.897(4)	1.870(2)
Mn(2)–N(39)	1.981(3)	1.982(5)	1.977(2)
Mn(2)–N(42)	1.982(3)	1.980(5)	1.988(2)
Mn(2)–O(83)	2.137(3)	2.127(4)	2.089(2)
O(11)–Mn(1)–O(30)	94.4(1)	94.5(2)	94.2(1)
O(11)–Mn(1)–N(19)	92.5(1)	91.8(2)	92.3(1)
O(30)–Mn(1)–N(19)	166.1(1)	166.6(2)	165.5(1)
O(11)–Mn(1)–N(22)	173.1(1)	173.5(2)	174.3(1)
O(30)–Mn(1)–N(22)	89.4(1)	89.6(2)	89.4(1)
N(19)–Mn(1)–N(22)	82.6(1)	83.3(2)	83.2(1)
O(11)–Mn(1)–O(81)	97.9(1)	96.9(2)	97.2(1)
O(30)–Mn(1)–O(81)	96.6(1)	98.6(2)	95.3(1)
N(19)–Mn(1)–O(81)	94.4(1)	92.4(2)	96.7(1)
N(22)–Mn(1)–O(81)	87.4(1)	87.5(2)	86.9(1)
O(31)–Mn(2)–O(50)	93.3(1)	94.0(2)	90.8(1)
O(31)–Mn(2)–N(39)	92.0(1)	92.2(2)	91.5(1)
O(50)–Mn(2)–N(39)	166.5(1)	165.2(2)	165.8(1)
O(31)–Mn(2)–N(42)	167.8(1)	167.9(2)	154.7(1)
O(50)–Mn(2)–N(42)	90.0(2)	89.6(2)	90.6(1)
N(39)–Mn(2)–N(42)	82.4(1)	81.7(2)	81.5(1)
O(31)–Mn(2)–O(83)	104.2(1)	99.8(2)	104.9(1)
O(50)–Mn(2)–O(83)	96.7(1)	94.5(2)	99.9(1)
N(39)–Mn(2)–O(83)	94.0(1)	97.7(2)	93.1(1)
N(42)–Mn(2)–O(83)	94.0(1)	91.5(2)	99.8(1)
Mn(1)···O(30)[a]	2.543(2)	2.576(4)	2.493(2)
Mn(2)···O(50)[b]	2.743(3)	2.729(4)	3.621(2)
Mn(1)···Mn(1)[a]	3.361(11)	3.387(2)	3.364(1)
Mn(2)···Mn(2)[b]	3.497(12)	3.525(2)	4.087(1)
Mn1···Mn2	5.749	5.737	5.478

Symmetry codes, a: 1 – *x*, 1 – *y*, –*z* (for **1** and **3**), 1 – *x*, –*y*, –*z* (for **2**); b: –*x*, –*y*, 1 – *z* (for **1**), 1 – *x*, 1 – *y*, 1 – *z* (for **2**), 1 –*x*, 2 – *y*, 1 – *z* (for **3**).

The root mean squared (r.m.s.) deviations of the four basal donor atoms from their mean planes around Mn(1) and Mn(2) are 0.053 and 0.004 Å, respectively. The Mn(1) and Mn(2) ions deviate from their respective mean planes by 0.144(1) and 0.194(1) Å, respectively, and do so in the direction of the bridging axial carboxylate oxygen atom. The planes intersect at an angle of 54.9(9)°.

In addition to these five strong bonds, the metal ions show weak interactions, at the other axial positions, with the phenoxo oxygen atoms of salen ligands on neighboring dinuclear units, with Mn(1)–O(30)[a] 2.543(2) Å (a: 1 – *x*, 1 – *y*, –*z*) and Mn(2)–O(50)[b] 2.743(3) Å (b: –*x*, –*y*, 1 – *z*) thus forming centrosymmetric bridging arrangements as shown in Figure 2. These two alternating bridging systems, i.e. phenoxo- and *syn-anti* carboxylate, constitute the one-dimensional chain structure of this compound. The two associated (phenoxo-bridged) Mn···Mn distances are 3.361(11) and 3.497(12) Å, and the distance between the carboxylate-bridged Mn ions [Mn(1)···Mn(2)] is 5.749(3) Å.

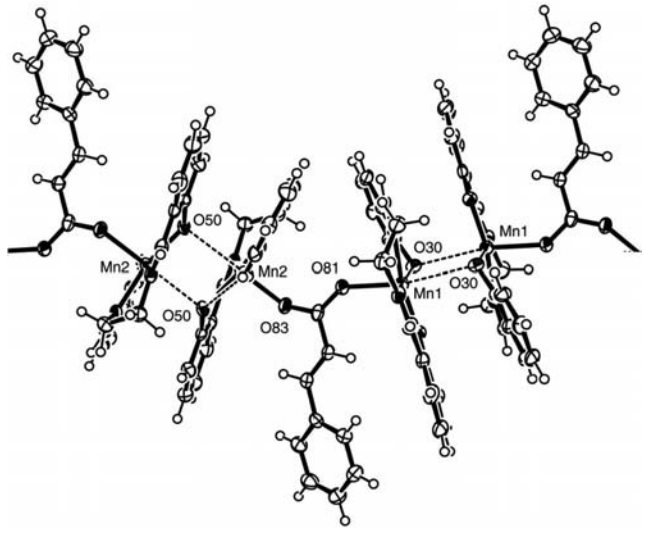

Figure 2. A view of the polymeric structure of complex **1**. Ellipsoids are drawn at the 30% probability level. The weak Mn(2)–O(50) and Mn(1)–O(30) interactions are shown as dotted lines.

The crystal packing of complex **1** is further stabilized by offset or slipped stacking π···π interactions (Figure S2, Supporting Information). The phenyl rings of the carboxylate-bridged dimeric units are stacked with respect to each other [ring R1: C(32)–C(33)–C(34)–C(35)–C(36)–C(37) with ring R2: C(44)–C(45)–C(46)–C(47)–C(48)–C(49)] with a centroid–centroid distance of 3.728(2) Å (Figure S2, Supporting Information). The π···π interactions are quite strong because the dihedral angle between the rings is 14.3° with a slip angle of 21.3°. Similarly, the phenyl rings R3 [C(24)–C(25)–C(26)–C(27)–C(28)–C(29)] and R4 [C(12)–C(13)–C(14)–C(15)–C(16)–C(17)] are also stabilized by π···π interactions with a centroid–centroid distance of 3.611(2) Å and the dihedral angle between the rings is 11.6° and the slip angle is 17.9°.

$\{[Mn_2(salen)_2(OPh)](ClO_4)\}_n$ (2). The structure of **2**, shown in Figure 3, is similar to that of **1**. Bond lengths, listed in Table 1, are also similar with the Mn–O(salen) bond lengths within the range 1.856(4)–1.868(4) Å, Mn–N 1.978(4)–1.982(5) Å, and Mn–O(carboxylate), with the ligand in the axial position, 2.110(4)–2.127(4) Å. The r.m.s.

deviations of the four basal donor atoms from their mean planes around Mn(1) and Mn(2) are 0.059 and 0.015 Å, respectively. The Mn(1) and Mn(2) ions deviate from these mean planes by 0.136(2) and 0.200(1) Å, respectively, and do so in the direction of the bridging axial carboxylate oxygen atom. The planes intersect at an angle of 58.7(1)°.

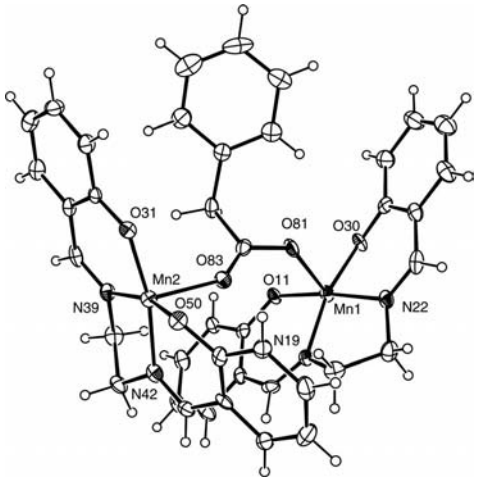

Figure 3. The dimeric structure of **2** with ellipsoids drawn at the 30% probability level.

The packing of the dimers in **2** to form a 1-dimensional polymer is also similar to that in **1**, as shown in Figure 4. The weak axial interactions are Mn(1)–O(30)[a] 2.576(4) Å (a: 1 – *x*, –*y*, –*z*) and Mn(2)–O(50)[b] 2.729(4) Å (b: 1 – *x*, 1 – *y*, 1 – *z*) and the two Mn···Mn distances are 3.387(2) and 3.525(2) Å. The Mn(1)···Mn(2) distance within the dinuclear unit is 5.737(3) Å. In addition to the weak phenoxo bridge, the dinuclear units are also stacked with respect to each other and stabilized by π···π interactions between the phenyl rings [ring R1: C(24)–C(25)–C(26)–C(27)–C(28)–C(29) with ring R2: C(12)–C(13)–C(14)–C(15)–C(16)–C(17)] with a centroid–centroid distance of 3.663(4) Å (Figure S3, Supporting Information); the dihedral angle between the rings is 10.7° and the slip angle is 22.6°. Similarly,

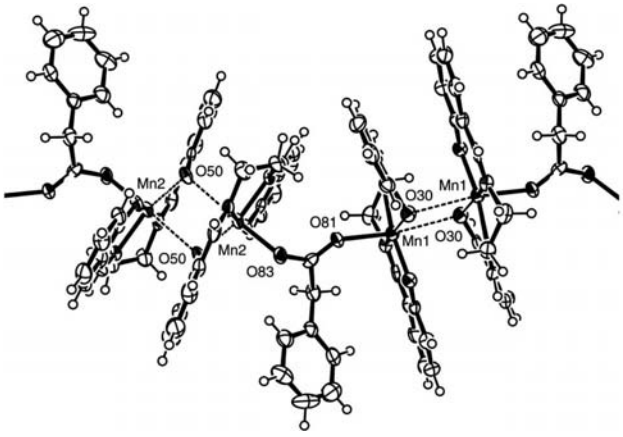

Figure 4. A view of the polymeric structure of complex **2**. Ellipsoids are drawn at the 30% probability level. The weak Mn(2)–O(50) and Mn(1)–O(30) interactions are shown as dotted lines.

the phenyl rings R3 [C(44)–C(45)–C(46)–C(47)–C(48)–C(49)] and R4 [C(32)–C(33)–C(34)–C(35)–C(36)–C(37)] are also stabilized by π–π interactions with a centroid–centroid distance of 3.733(3) Å and with a dihedral angle between the rings of 15.0° and a slip angle of 22.6°. In this compound there is a short Csp^2–H···π (phenyl) contact between C(86)–H(68) and a phenyl group of the salen molecule (Figure S3, Supporting Information), where the H(86)···Cg(R4) distance is 2.71 Å and the C(86)–H(86)···Cg(R4) angle is 141° (Cg: centroid of the phenyl ring).

{[Mn_2(salen)$_2$(OBz)][ClO_4)}$_2$ (3). The structure of **3** is also a dimer, as shown in Figure 5. In this compound the equatorial planes of the metal complexes are approximately planar, with the r.m.s. deviations of the four donor atoms from their mean planes around Mn(1) and Mn(2) being 0.074 Å and 0.098 Å, respectively. The Mn(1) and Mn(2) ions deviate from these mean planes by 0.141(1) and 0.319(1) Å, respectively, and deviate towards the bridging axial benzoate oxygen atom. The planes intersect at an angle of 62.0(1)°. It may be noted that the angles between the planes can be correlated with the steric bulks of the bridging carboxylate ligands, thus the angle is smallest in **1** with cinnamate and largest in **3** where the aromatic ring of the carboxylate is close to the metal coordination spheres. The bond lengths are as expected for Mn–O (ligand) and are in the range 1.856(4)–1.868(4) Å, Mn–N 1.978(4)–1.982(5) Å, and for Mn–O(carboxylate) where the ligand is in the axial position, the distances are within the range 2.110(4)–2.127(4) Å.

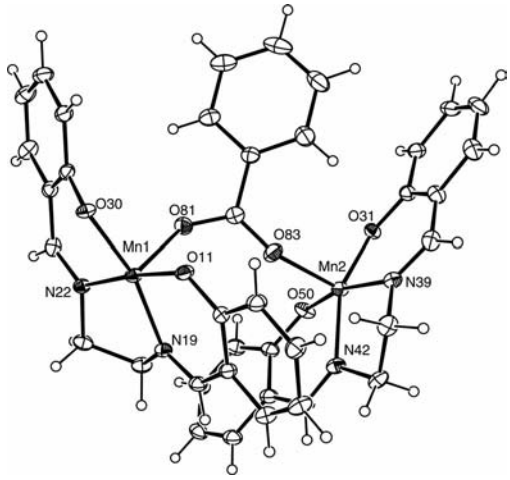

Figure 5. The dimeric structure of **3** with the ellipsoids drawn at the 30% probability level.

The packing of the dimers in the crystal structure of **3** is however somewhat different than in **1** and **2**, as O(30)[a] is 2.493(2) Å from the vacant axial position on Mn(1) and O(50)[b] is 3.621(2) Å from Mn(2). In no way can this latter distance be considered even as a weak interaction, and therefore **3** is best considered to be a tetramer, as shown in Figure 6. The associated Mn···Mn distances are 3.364(1) and 4.087(1) Å. The distance between Mn(1) and Mn(2) within the carboxylate-bridged dimeric unit is 5.478(3) Å. As in **1** and **2**, in addition to phenoxo bridges, two dinuclear

units are also held together by π···π interactions (Figure S4, Supporting Information) between phenyl rings R1 and R2 of the salen ligands [R1: C(24)–C(25)–C(26)–C(27)–C(28)–C(29), R2: C(12)–C(13)–C(14)–C(15)–C(16)–C(17)] with a centroid–centroid distance of 3.806(19) Å, and a dihedral angle between the rings of 14.3° and a slip angle of 26.0°.

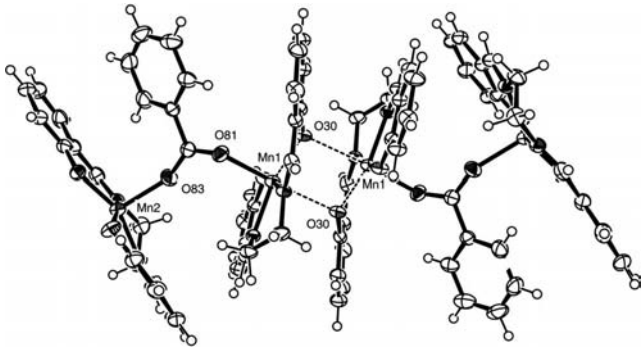

Figure 6. A view of the tetrameric structure of complex **3**. Ellipsoids are drawn at the 30% probability level. The weak Mn(1)–O(30) interactions are shown as dotted lines.

A search of the CCDC database shows that only two compounds similar to those reported herein, $[Mn_2(salen)_2(CH_3COO)]ClO_4$[16] and $[Mn_2(7\text{-Me-salen})_2(CH_3COO)]ClO_4$[17] are known. Both of these compounds are reported to be acetate-bridged dimers. The association of the dimeric units via the phenoxo bridge of any of these complexes was not analyzed, although the deposited CIF associated with ref.[16] (for ref.[17] the atomic coordinates for the reported structures are not deposited) reveals that it is a 1D polymer like **1** and **2** with long Mn–O(ligand) distances, 2.453 and 2.686 Å, involving the vacant axial positions of the metal coordination sphere. The magnetic properties of these complexes were not explored.

Magnetic Study for Compounds 1, 2 and 3

We measured the magnetic properties of **1**–**3** on a SQUID magnetometer with an applied field of 0.5 T. These compounds consist of dimeric motifs, and the magnetization and susceptibility were analyzed based on the Mn_2 environments. The $\chi_m T$ vs. T plot for **1** is shown in Figure 7 (a) (where χ_m = molar magnetic susceptibility). In the high-temperature region (≥20 K), the data obeyed the Curie–Weiss law, $\chi_m = C/(T - \theta)$, where C is the Curie constant and θ is the Weiss temperature. The parameters were optimized to give $C = 5.93(2)\ cm^3\,K\,mol^{-1}$ and $\theta = -2.0(2)$ K. The value of C is close to the spin-only value of $6.0\ cm^3\,K\,mol^{-1}$ that is expected for two high-spin d^4 (S = 2) contributions. The g value of **1** was 1.99. The g value is

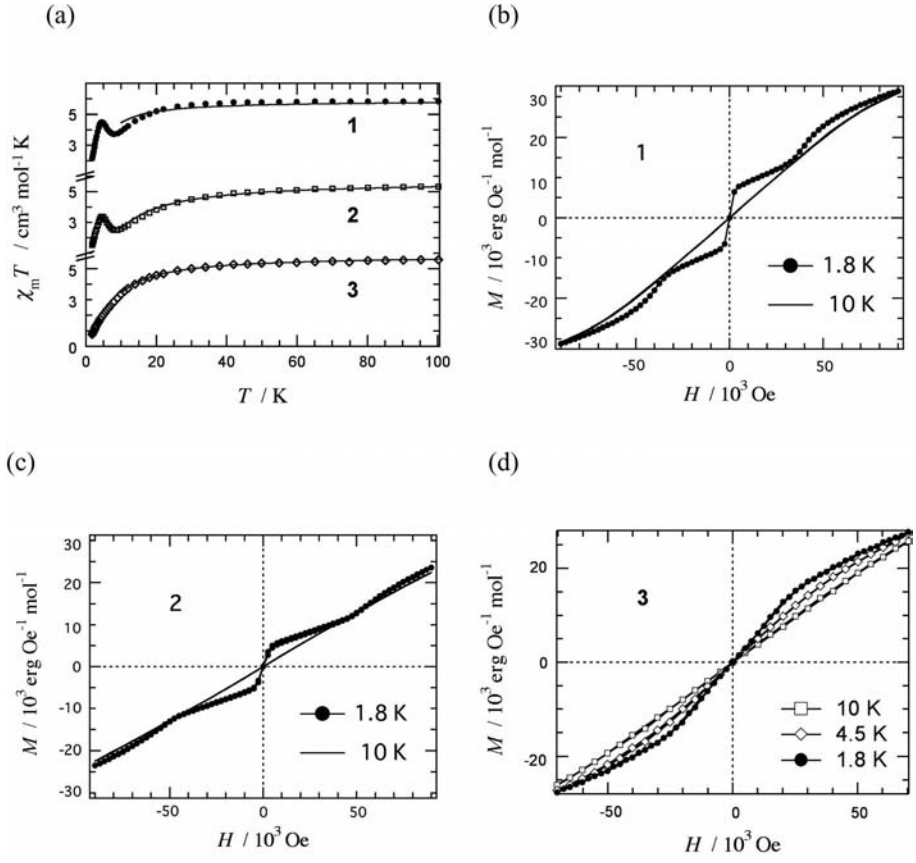

Figure 7. (a) The $\chi_m T$ vs. T plot for a randomly oriented polycrystalline specimens of **1**– **3**. Solid lines are the best fit to Equation 2. See the text for optimized fitting parameters; magnetization–magnetic field strength (M–H) curves for polycrystalline **1** (b) and **2** (c) measured at 1.8 and 10 K; (d) M–H curves for polycrystalline **3** measured at 1.8, 4.5, and 10 K. Lines are drawn as a guide.

very slightly smaller than 2, which is often observed for high-spin Mn^{3+} compounds.[18] On cooling, the $\chi_m T$ value decreased, but a small hump was observed in the data at ca. 4.5 K. This behavior was well reproduced, without any thermal hysteresis, after heating and cooling of the sample.

As Figure 7 (b) shows, the magnetization (M) of **1** measured at 10 K displayed almost linear field dependence. On the other hand, significant excess magnetization at ca. 1 T was recorded at 1.8 K. A $\chi_m T$–T anomaly is related to a M–H curve anomaly, and this excess magnetization is responsible for the cusp in the $\chi_m T$–T curve (Figure 7, a). At higher applied fields, the magnetization behavior became identical to that recorded at 10 K, implying that the specimen violated the Curie–Weiss law. The excess magnetization was almost constant over the 1.8–3 K range (see Figure S1, Supporting Information). The constant dM/dH slope gives rise to a $\chi_m T$ value proportional to T, which is in agreement with the final drop below 4.5 K in the $\chi_m T$ vs. T plot. The magnetization at 9 T (3.2×10^4 erg Oe^{-1} mol^{-1}) was considerably smaller than the theoretical saturation magnetization (4.5×10^4 erg Oe^{-1} mol^{-1}). The very small slope implies the presence of dominant antiferromagnetic interactions in this system. No magnetic hysteresis was observed.

The magnetic behavior of **2** is similar to that of **1**. The $\chi_m T$ vs. T plot for **2** showed Curie–Weiss behavior in the high temperature region [C = 5.77(3) cm^3 K mol^{-1}, g = 1.96, and θ = –8.6(4) K for $T \geq 20$ K]. A $\chi_m T$ peak was found at ca. 4.5 K. The M–H curves for **2** were also similar to those of **1** (Figure 7, c); almost linear field dependence was observed for the data recorded at 10 K, whereas an additional magnetization was superposed at ca. 1 T on the data curve recorded at 1.8 K. In contrast to the results of **1** and **2**, the $\chi_m T$ vs. T plot of **3** exhibited no anomaly (Figure 7, a). The $\chi_m T$ value for this sample monotonically decreased upon cooling. The Curie–Weiss analysis of the 20–300 K data afforded C = 5.90(2) cm^3 K mol^{-1}, g = 1.98, and θ = –5.5(1) K. The magnetization curves imply the presence of appreciable antiferromagnetic coupling in **3** (Figure 7, d). From a close look at the magnetization curve recorded at 1.8 K, we see an indication of inflated magnetization in addition to a Brillouin-type curve. This phenomenon was also observed in the data for **1** and **2**, but because the temperature at which the anomaly can be observed is much lower for **3** the magnitude of the interaction in this specimen is smaller than for **1** and **2**.

To investigate the presence of a magnetic phase transition we measured FCM, remnant magnetization (RM), and zero-field-cooled magnetization (ZFCM) data for **1**, **2**, and **3** (Figure 8, a). In the data for **1** a clear field-cooled magnetization (FCM) peak was found at 4.0 K. No RM was observed. The ZFCM and FCM curves for **1** coincide with each other. Accordingly, we can confirm that the data for this specimen showed no hysteresis. The data for compound **2** also showed no hysteresis, and a clear peak was found at 4.6 K in the FCM and ZFCM curves. These findings suggest that the specimens undergo antiferromagnetic phase transitions at the temperatures at which the peaks were observed in their data. On the other hand, compound **3** showed no peak in its FCM or ZFCM data, and no RM was recorded, indicating that **3** is a paramagnet down to 1.8 K.

Alternating current (ac) magnetometry is a versatile tool for determining a magnetic phase transition temperature, and for investigating single-molecule and single-chain mag-

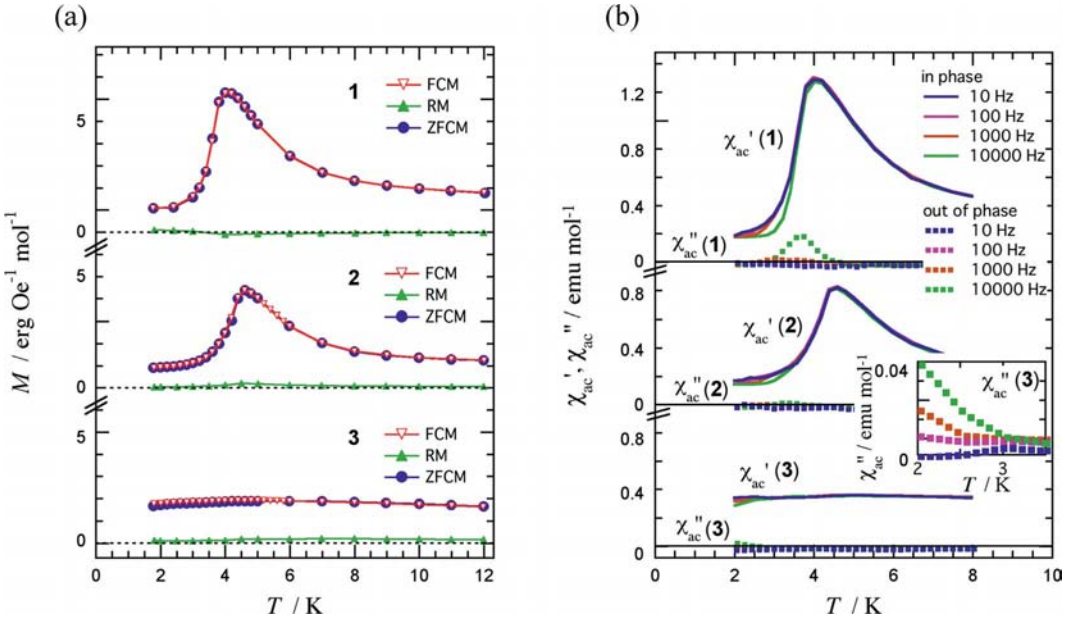

Figure 8. (a) The FCM, RM, and ZFCM results for polycrystalline **1**–**3**. FCM was measured at 5 Oe upon cooling, RM at zero field upon heating after the FCM measurements, and ZFCM at 5 Oe upon heating. The FCM and ZFCM data almost coincide; (b) The ac magnetic susceptibility curves, χ_{ac}' (in-phase) and χ_{ac}'' (out-of-phase), for **1**–**3**. The ac field was applied with an amplitude of 5 Oe and frequencies of 10–10000 Hz. Solid and dotted lines are guides. Inset shows an expansion of the low temperate region of the χ_{ac}'' curve for **3**.

nets that show slow magnetization reversal.[19] The ac magnetic susceptibilities of **1**–**3** were measured (Figure 8, b), and we confirmed that **1** and **2** showed antiferromagnetic phase transitions (T_N) at 4.0 and 4.6 K, respectively, whereas **3** did not. The in-phase portion (χ_{ac}') of the curves for **1**–**3** follow practically the same profiles as the curves recorded in the FCM and ZFCM measurements. The peak positions did not alter regardless of frequency, indicating that both **1** and **2** are not single-chain/molecule magnets, super-paramagnets, or spin-glasses. When a fast ac frequency was applied a small, but meaningful, peak was observed at 3.5 K in the out-of-phase portion (χ_{ac}'') of the data for **1**. Similar behavior was found at 3.2 K in the data for **2**, but the peak is much smaller even at 10000 Hz. The temperature at which the data for **1** and **2** become frequency-dependent is lower than T_N. This may be due to the fact that there is possibly an activation energy associated with the movement of the magnetic domain boundary.[20,21] Compound **3** exhibited a decrease in χ_{ac}' and a concomitant increase in χ_{ac}'' at ca. 2 K when the ac frequency was elevated. Although this frequency dependence is small, this finding seems to indicate that **3** shows slow magnetization reversal that is characteristic of single-molecule/single-chain magnets (Figure 8, b, inset).

All the compounds showed a distinct $\chi_m T$ decrease below ca. 30 K, which indicates the presence of dominantly antiferromagnetic couplings in all of them, but residual magnetic moments of **1** and **2** were present below the T_N, as indicated by the small hump in the magnetization curves for these complexes. This observation can be explained plausibly in terms of spin canting (Figure 9). The canting angles for these complexes can be estimated from the residual moments by the extrapolation of the magnetization curves as $H \rightarrow 0$. The residual moment of 5.7×10^3 erg Oe^{-1} mol^{-1} for **1** afforded a cant angle of 7.3°, and for **2** the residual moment of 3.6×10^3 erg Oe^{-1} mol^{-1} gave a cant angle of 4.6°.

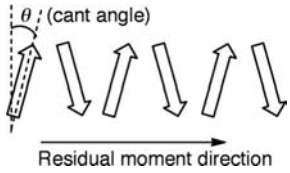

Figure 9. Schematic drawing of spin canting.

The magnetic exchange coupling leads only to a parallel or antiparallel spin alignment, and therefore the origin of the driving force for the spin canting is worthy of discussion. The Dzyaloshinskii–Moriya (DM) interaction[22,23] is expressed as $D_{DM} \cdot (S_i \times S_j)$ where the constant vector D_{DM} is approximately proportional to $(\Delta g/g)J$ (where J = exchange interaction constant), and Δg is the deviation of g from 2.[23] In general, spin-orbit coupling affects Δg and D_{DM}, and Mn^{3+} coordination compounds may exhibit appreciable DM antisymmetric exchange despite g being nearly equal to 2. The importance of bridging ligands in destroying the centrosymmetry between neighboring spins has been noted[24] e.g. the bridges in low-dimensional magnets such as carboxylate ligands[25] (like in the present study), azide,[24,26] and pyrimidine.[27,24]

There are two reasons for spin canting, one is the DM interaction and the other is single-ion anisotropy.[25,28] Manganese(III) compounds often exhibit pronounced magnetic anisotropy defined by a negative D value (where D is the zero-field splitting parameter) in Equation (1) due to Jahn–Teller distortion of the metal coordination sphere. The z-axis is defined as the magnetic easy axis at each ion.

$$\hat{H} = D\left[\hat{S}_z^2 - \frac{1}{3}S(S+1)\right] \quad (1)$$

There are two crystallographically independent manganese ions in the unit cells of **1** and **2**, and the axial direction on the ions is canted in a zigzag manner along the chain. Such conditions will bring about a spin-canted structure as a result of a combination of antiferromagnetic coupling and strong anisotropy.[24–28] The carboxylate bridge causes the neighboring coordination basal planes to intersect at angles of 54.9(1) and 58.7(1)° for **1** and **2**, respectively, which implies a theoretical maximum cant angle of 27–29°. The presence of antiferromagnetic coupling across the carboxylate groups is responsible for the small cant angles. In the case where single-ion magnetic anisotropy is operative, we have to pay attention to the fact that the DM interaction is always operative at the same time because the lack of centrosymmetry is favorable for DM interactions. However, only the large magnetic anisotropy can explain the spin dynamics observed in **1** and **2** (Figure 8, b).

In a small applied field the canted antiferromagnetic phases of **1** and **2** are in the ground state, but on applying a field of > 3 Tgenuine antiferromangetic character becomes strong in these specimens. This feature is different from the behavior of ordinary canted antiferromagnets, since conventional canted antiferromagnets usually exhibit linear field dependence with increasing applied field.[22,23,28] Furthermore, we find another broad hump around 6–7 T in parts b and c of Figure 7; a simple spin-canting model cannot explain these additional increases or decreases in magnetization. One possible reason for these humps in the data is the competing interaction between the zero-field splittings and the magnetic couplings that have different amplitudes.[29] These features seem to be characteristic of the hierarchical interactions that are due to the low dimensionality of the structures.

This semi-quantitative analysis of the exchange parameters and magneto-structural relationship requires further comment. It is well known that carboxylate anions play a role as an antiferromagnetic coupler for various transition metal ions including Mn^{3+}.[30,31] This bridging structures have been classified based on *syn* and *anti* configurations,[31] and *syn-anti* bridges, as found in **1**, **2** and **3**, are reported to transmit antiferromagnetic coupling.[30] The largest coupling (J_1) may be attributed to the caroxylato linkage, despite the Mn···Mn distance being longer than that of the

$$\chi_m = \frac{2Ng^2\mu_B{}^2}{k_BT}\frac{30+14\exp(-8J/k_BT)+5\exp(-14J/k_BT)+\exp(-18J/k_BT)}{9+7\exp(-8J/k_BT)+5\exp(-14J/k_BT)+3\exp(-18J/k_BT)+\exp(-20J/k_BT)} \quad (2)$$

phenoxo linkage. The double Mn–O(phenoxo)–Mn* linkages possess centrosymmetry that is incompatible with the canted spin structure.

A numerical analyses of the high temperature regions of the χ_mT vs. T plots for **1**–**3** can give information pertaining to the largest J parameter for these complexes. Such an approximation is needed because there are too many parameters to enable a complete analysis to be performed. A simple antiferromagnetic model can be use to estimate the dominant antiferromagnetic interaction in canted antiferromagnets. The values of J_1 were estimated for **1**–**3** from the χ_mT vs. T data for $T \geq 10$ K on the basis of a nearest-neighboring $S = 2$ dinuclear model with the Heisenberg spin-Hamiltonian $H = -2J_1\ S_1{\cdot}S_2$. By using Equation (2) we obtained $J_1/k_B = -0.41(4)$, $-1.58(3)$, and $-1.11(1)$ K for **1**, **2**, and **3**, respectively.

We attempted to estimate J_1 more precisely by introducing the parameter D into the analyses.[33] However, the optimized parameters were unrealistic when compared with the typical values for dinuclear Mn^{3+} complexes,[33c] presumably because of possible over-parameterization of the small and monotonic decrease of the χ_mT vs. T profiles down to 10 K.

The axial Mn–O(phenoxo)–Mn* linkage can aid ferromagnetic coupling (defined by the coupling parameter J_2). If the ferromagnetic interaction across the phenoxo bridge was dominant in these complexes, the χ_mT value would show an increase upon cooling of the compounds. Therefore, for **1**–**3** J_2 is semi-quantitatively determined to be smaller in absolute magnitude than J_1.

Several oxo-bridged dinuclear Mn^{3+} systems are known to possess ground high-spin states.[32] Furthermore, a number of dinuclear Mn^{3+} compounds with salen-based ligands have been characterized as ground high-spin molecules.[5,6] The first reported single-chain magnet, $[Mn^{3+}{}_2Ni^{2+}]$, also involves ferromagnetically related salen-based Mn_2 building blocks.[34] These reports support our hypothesis that ferromagnetic Mn–O–Mn* coupling is present in compounds **1**–**3**. Note that isolated dinuclear Mn^{3+} building blocks involving salen-based bridges are known to be potential single-molecule magnets.[6a] It can be concluded that the relatively large inter-block interactions (J_1) in **1** and **2** are unfavorable for the development of single-molecule magnets. The canted spin structure forms before they can behave as single-molecule magnets.

Compounds **1** and **2** must have an interchain magnetic interaction because they exhibited long-range magnetic order. The ground states of **1** and **2** are antiferromagnetic, and accordingly the interchain interaction should be antiferromagnetic for the magnetic chains that have relatively small moments due to spin canting. Therefore, the order of the exchange couplings can be concluded to be as follows: $|J_1$ (canted antiferro.)$| > |J_2$ (ferro.)$| > |J_{interchain}$ (antiferro.)$|$.

Compound **3** showed no peak in its FCM or χ_{ac}' data. The magnetization and the ac in-phase susceptibility remained constant down to 1.8 K and finally exhibited frequency dependence around 2 K, as shown in Figure 8 (b, inset). Therefore, the coupling J_1 (canted antiferro.) is operative in Mn(1)–O–C–O–Mn(2) resulting in a residual moment per dinuclear unit. On the other hand, J_2 is negligible or absent in Mn–O–Mn*. Each dinuclear unit is magnetically isolated; that is, the residual moments form approximately ideal paramagnets in the units. The observed Mn–O(phenoxo) distance in **3** [3.621(2) Å], which is relatively long compared with those in **1** and **2**, is consistent with this argument. In summary, the present study of series **1**–**3** provides a typical discussion of the magneto-structure relationship; the Mn–O–Mn* distance is an important and sensitive variable, not only for intrachain magnetic coupling, but also for bulk magnetism and single-molecule/single-chain magnet behavior.

Conclusions

We have synthesized, by varying the carboxylate group, three very rare alternating carboxylate- and phenoxo-bridged Mn^{III} complexes of salen. The crystal structures reveal that in all three complexes the bridging mode of the carboxylate remains the same (*syn-anti*), but the angle of intersection between the two equatorial planes of the carboxylate-bridged Mn^{III} ions varies systematically. This variation seems to have appreciable effect on the association of the dinuclear molecules through axial Mn···O(phenoxo) interactions to form the 1D chain structure; in **3**, in which the intersection angle is the largest, propagation of chain is terminated after each tetranuclear entity. From the magnetic point of view, the present systems have been shown to possess two types of magnetic ground states as a result of the balance between antiferromagnetic and ferromagnetic couplings in the alternating $S = 2$ chains, which in turn depend upon the geometries of the Mn–O(phenoxo)–Mn and Mn–O–C–O–Mn bridges. The assignment of magnetic couplings to the geometrical structures has been proven by taking into consideration a spin-canted arrangement in the structures. Compounds **1** and **2** exhibit long-range order, and the origin of the magnetic moments is due to the spin canting. Unfortunately, the compounds **1**–**3** do not show hysteresis above 2 K as would be expected for a single-molecule/single-chain magnet. The Mn_2 building block is versatile, and the present study informs us that attention must be paid to the competition between intra- and inter-block interactions. The latter is unexpectedly larger than the former in the case of the materials reported herein.

Experimental Section

Starting Materials: Salicylaldehyde, 1,2-ethanediamine, benzoic acid (HOBz), phenyl acetic acid (HOPh) and cinnamic acid

(HOCn) were purchased from commercial sources and used as received. All other solvents were of reagent grade and were used without further purification.

Caution! *Perchlorate salts of metal complexes with organic ligands are potentially explosive. Only small amounts of material should be prepared and handled with great care.*

Schiff-base Ligand *N,N′*-Bis(salicylidene)-1,2-diaminoethane (H_2salen): The tetradentate Schiff-base ligand was prepared by the condensation of salicylaldehyde (1.05 mL, 10 mmol) and 1,2-ethanediamine (0.31 mL, 5 mmol) in methanol (10 mL).

{[Mn_2(salen)$_2$(OCn)](ClO$_4$)}$_n$ (1), {[Mn_2(salen)$_2$(OPh)](ClO$_4$)}$_n$ (2) and {[Mn_2(salen)$_2$(OBz)](ClO$_4$)}$_2$ (3): A methanolic solution (10 mL) of the ligand H_2salen (5 mmol) was added to a methanolic solution (10 mL) of $Mn(ClO_4)_2{\cdot}6H_2O$ (1.805 g, 5 mmol) with constant stirring. After ca. 15 min methanolic solutions (5 mL) of cinnamic acid (for **1**) (0.370 g, 2.5 mmol), phenyl acetic acid (for **2**) (0.340 g, 2.5 mmol) and benzoic acid (for **3**) (0.305 g, 2.5 mmol) were added to the salen mixtures. Triethylamine (0.35 mL, 2.5 mmol) was added drop wise to each of the solutions with constant stirring. The color of all the solutions turned to dark brown immediately. Slow evaporation of the resulting brown solutions gave dark brown microcrystalline **1**–**3**. Once the volume of the solutions were reduced to ca. 10 mL, the solids were filtered off and washed with diethyl ether, and then redissolved in CH_3CN for **1** and in CH_3OH for **2** and **3**. Layering these brown solutions with Et_2O gave well formed X-ray quality single crystals.

Complex 1: Yield 1.39 g; 63%. $C_{41}H_{35}ClMn_2N_4O_{10}$ (889.06): calcd. C 55.39, H 3.97, N 6.30; found C 55.48, H 3.89, N 6.38. IR (KBr pellet): $\tilde{\nu}$ = 1621 [ν(C=N)], 1534 [ν_{as}(C=O)], 1441 [ν_s(C=O), $\nu(ClO_4^-)$], 1098 cm^{-1}. λ_{max} (nm) and ε_{max} (dm^{3}mol^{-1}) (CH_3CN solution): 398 and 917.

Complex 2: Yield 1.51 g; 69%. $C_{40}H_{35}ClMn_2N_4O_{10}$ (877.05): calcd. C 54.78, H 4.02, N 6.39; found C 54.84, H 4.10, N 6.45. IR (KBr pellet): $\tilde{\nu}$ = 1619 [ν(C=N)], 1543 [ν_{as}(C=O)], 1438 [ν_s(C=O), $\nu(ClO_4^-)$], 1094 cm^{-1}. λ_{max} (nm) and ε_{max} (dm^{3}mol^{-1}) (CH_3CN solution): 395 and 930.

Complex 3: Yield 1.61 g; 75%. $C_{39}H_{33}ClMn_2N_4O_{10}$ (863.02): calcd. C 54.28, H 3.85, N 6.49; found C 54.37, H 3.97, N 6.56. IR (KBr pellet): $\tilde{\nu}$ = 1618 [ν(C=N)], 1534 [ν_{as}(C=O)], 1440 [ν_s(C=O), $\nu(ClO_4^-)$], 1098 cm^{-1}. λ_{max} (nm) and ε_{max} (dm^{3}mol^{-1}) (CH_3CN solution): 391 and 965.

Physical Measurements: Elemental analyses (C, H and N) were performed with a Perkin–Elmer 240C elemental analyzer. IR spectra in KBr (4500–500 cm^{-1}) were recorded with a Perkin–Elmer RXI FT-IR spectrophotometer. The electronic absorption spectra (1000–200 nm) of the complexes were recorded in CH_3CN with a Hitachi U-3501 spectrophotometer.

Static (direct current) magnetic susceptibilities on polycrystalline samples of **1**–**3** were measured on a Quantum Design SQUID magnetometer (MPMS-7) with applied magnetic fields of 5000 and 500 Oe over a temperature range of 1.8–300 K. Typical sample masses were 20–50 mg. The magnetic response was corrected with diamagnetic blank data recorded for the empty sample holder. The diamagnetic contribution of the sample itself was estimated from Pascal's constant. The magnetization curves were recorded from –70 to +70 kOe. The alternating current magnetic susceptibilities were obtained on a Quantum Design PPMS ac/dc magnetometer with polycrystalline samples. The ac frequency was varied from 10 to 10000 Hz with an amplitude of 5 Oe. Hysteresis curves at 9 T were recorded on the PPMS magnetometer. The magnetization was calibrated with the SQUID results.

Crystallographic Studies: Crystal data for the three crystals are given in Table 2. For **1**, **2** and **3**, 10199, 10076, 9809 independent data were collected, respectively, with Mo-K_α radiation at 150 K with an Oxford Diffraction X-Calibur CCD System. The crystals were positioned 50 mm from the CCD detector. A total of 321 frames were measured for each crystal with a counting time of 10 s per frame. Data analyses were carried out with the CrysAlis program.[35] The structures were solved by direct methods with the SHELXS97 program.[36] The non-hydrogen atoms were refined with anisotropic thermal parameters. The hydrogen atoms bonded to C atoms were included in the refinement model at geometric positions and given thermal parameters equivalent to 1.2 times

Table 2. Crystal data and structure refinement details for complexes **1**–**3**.

	1	**2**	**3**
Formula	$C_{41}H_{35}ClMn_2N_4O_{10}$	$C_{40}H_{35}ClMn_2N_4O_{10}$	$C_{39}H_{33}ClMn_2N_4O_{10}$
Formula weight	889.06	877.05	829.65
Space group	$P\bar{1}$	$P\bar{1}$	$P\bar{1}$
Crystal system	triclinic	triclinic	triclinic
a [Å]	10.3388(7)	10.207(3)	10.090(3)
b [Å]	13.6814(10)	13.581(3)	13.318(2)
c [Å]	14.5854(9)	14.380(4)	14.441(3)
α [°]	72.555(6)	100.70(2)	100.803(14)
β [°]	69.831(6)	108.22(3)	107.32(2)
γ [°]	82.744(6)	99.90(2)	98.770(17)
V [Å^3]	1846.9(2)	1803.1(8)	1774.1(6)
Z	2	2	2
Calcd. density (D_{calc}) [g cm^{-3}]	1.599	1.615	1.616
Absorption coeff. (μ) [mm^{-1}]	0.825 (Mo-K_α)	0.843 (Mo-K_α)	0.856 (Mo-K_α)
F(000)	912	900	884
Crystal size [mm^3]	0.02 × 0.17 × 0.18	0.02 × 0.19 × 0.22	0.04 × 0.22 × 0.22
θ range [°]	2.37–30.00	2.17–30.00	2.65–30.0
R(int)	0.048	0.070	0.042
Unique data	10199	10076	9809
Data with $I > 2\sigma(I)$	4865	3322	5814
$R1$, wR_2	0.0617, 0.1236	0.0743, 0.1851	0.0508, 0.1176
GOF on F^2	0.811	0.736	0.866

those of the parent atoms. Absorption corrections for **1**, **2**, and **3** were carried out with the ABSPACK program.[37] The structures were refined on F^2 with SHELXL97.[36]

CCDC-788085 (for **1**), -788086 (for **2**) and -788087 (for **3**) contain the supplementary crystallographic data for this paper. These data can be obtained free of charge from The Cambridge Crystallographic Data Centre via www.ccdc.cam.ac.uk/data_request/cif.

Supporting Information (see footnote on the first page of this article): *M–H* curves for polycrystalline **1** and **2**; supramolecular chain structure of complexes **1** and **2** and tetramer of complex **3** showing phenoxo bridges, π···π and CH···π interactions; crystal packing diagrams for complexes **1**, **2** and **3**; experimental and simulated powder X-ray diffraction patterns of complexes **1**, **2** and **3**.

Acknowledgments

Paramita Kar is thankful to the Council of Scientific and Industrial Research (CSIR), India, for research fellowship [sanction number 09/028(0733)/2008-EMR-I]. We thank Engineering and Physical Sciences Research Council (EPSRC) and the University of Reading for funds for the X-Calibur system. We also are thankful for financial support by the Ministry of Education, Culture, Sports, Science and Technology, Japan (grant numbers 21110513 and 22350059).

[1] a) G. E. Kostakis, A. M. Ako, A. K. Powell, *Chem. Soc. Rev.* **2010**, *39*, 2238–2271, and references cited therein; b) H.-L. Sun, Z.-M. Wang, S. Gao, *Coord. Chem. Rev.* **2010**, *254*, 1081–1100, and references cited therein; c) Y.-F. Zeng, X. Hu, F.-C. Liu, X.-H. Bu, *Chem. Soc. Rev.* **2009**, *38*, 469–480; d) M. Kurmoo, *Chem. Soc. Rev.* **2009**, *38*, 1353–1379.

[2] J. J. R. Frausto da Silva, R. J. P. Williams, *The Biological Chemistry of the Elements*, Clarendon Press, Oxford, **1991**, pp. 370 (chapter 14).

[3] V. L. Pecoraro (Ed.), *Manganese Redox Enzymes*, VCH, New York, **1992**.

[4] H.-L. Shyu, H.-H. Wei, Y. Wang, *Inorg. Chim. Acta* **1999**, *290*, 8–13.

[5] H. Miyasaka, R. Clerac, W. Wernsdorfer, L. Lecren, C. Bonhomme, K.-I. Sugiura, M. Yamashita, *Angew. Chem. Int. Ed.* **2004**, *43*, 2801–2805.

[6] a) Z. Lu, M. Yuan, F. Pan, S. Gao, D. Zhang, D. Zhu, *Inorg. Chem.* **2006**, *45*, 3538–3548; b) H. Miyasaka, R. Clerac, T. Ishii, H. Chang, S. Kitagawa, M. Yamashita, *J. Chem. Soc., Dalton Trans.* **2002**, 1528–1534; c) H. Miyasaka, A. Saitoh, S. Abe, *Coord. Chem. Rev.* **2007**, *251*, 2622–2664.

[7] a) T. K. Maji, S. Sain, G. Mostafa, T.-H. Lu, J. Ribas, M. Monfort, N. R. Chaudhuri, *Inorg. Chem.* **2003**, *42*, 709–716; b) J. B. Vincent, H.-R. Chang, K. Folting, J. C. Huffman, G. Christou, D. N. Hendrickson, *J. Am. Chem. Soc.* **1987**, *109*, 5703–5711; c) J.-P. Zhao, B.-W. Hu, F. Lloret, J. Tao, Q. Yang, X.-F. Zhang, X.-H. Bu, *Inorg. Chem.* **2010**, *49*, 10390–10399.

[8] a) J. Pasan, J. Sanchiz, C. Ruiz-Perez, F. Lloret, M. Julve, *Eur. J. Inorg. Chem.* **2004**, 4081–4090 and references cited therein; b) F. S. Delgado, J. Sanchiz, C. Ruiz-Perez, F. Lloret, M. Julve, *Inorg. Chem.* **2003**, *42*, 5938–5948.

[9] Z.-L. Huang, M. Drillon, N. Masciocchi, A. Sironi, J.-T. Zao, P. Rabu, P. Panissod, *Chem. Mater.* **2000**, *12*, 2805–2812, and references cited therein.

[10] a) L. Pan, N. Ching, X. Huang, J. Li, *Inorg. Chem.* **2000**, *39*, 5333–5340; b) P. Mukherjee, M. G. B. Drew, C. J. Gomez-Garcia, A. Ghosh, *Inorg. Chem.* **2009**, *48*, 4817–4827; c) P. Mukherjee, M. G. B. Drew, C. J. Gomez-Garcia, A. Ghosh, *Inorg. Chem.* **2009**, *48*, 5848–5860.

[11] a) C. Biswas, P. Mukherjee, M. G. B. Drew, C. J. Gomez-Garcıa, J. M. Clemente-Juan, A. Ghosh, *Inorg. Chem.* **2007**, *46*, 10771–10780; b) A. K. Ghosh, D. Ghoshal, E. Zangrando, J. Ribas, N. R. Chaudhuri, *Inorg. Chem.* **2007**, *46*, 3057–3071; c) M. S. Ray, A. Ghosh, A. Das, M. G. B. Drew, J. Ribas-Ariño, J. Novoa, J. Ribas, *Chem. Commun.* **2004**, *4*,1102–1103.

[12] a) S. Konar, P. S. Mukherjee, M. G. B. Drew, J. Ribas, N. R. Chaudhuri, *Inorg. Chem.* **2003**, *42*, 2545–2552; b) C. Ruiz-Perez, J. Sanchiz, M. H. Molina, F. Lloret, M. Julve, *Inorg. Chem.* **2000**, *39*, 1363–1370; c) D. Armentano, G. De Munno, T. F. Mastropietro, D. M. Proserpio, M. Julve, F. Lloret, *Inorg. Chem.* **2004**, *43*, 5177–5179; d) H. Kumagai, C. J. Kepert, M. Kurmoo, *Inorg. Chem.* **2002**, *41*, 3410–3422; e) M.-H. Zeng, W.-X. Zhang, X.-Z. Sun, X.-M. Chen, *Angew. Chem. Int. Ed.* **2005**, *44*, 3079–3082.

[13] Z. Wang, B. Zhang, H. Fujiwara, H. Kobayashi, M. Kurmoo, *Chem. Commun.* **2004**, 416–417.

[14] Z. Wang, B. Zhang, M. Kurmoo, M. A. Green, H. Fujiwara, T. Otsuka, H. Kobayashi, *Inorg. Chem.* **2005**, *44*, 1230–1237.

[15] a) X.-Y. Wang, Z.-M. Wang, S. Gao, *Chem. Commun.* **2007**, 1127–1129; b) M. Viertelhaus, H. Henke, C. E. Anson, A. K. Powell, *Eur. J. Inorg. Chem.* **2003**, 2283–2289; c) M. Viertelhaus, P. Adler, R. Clerac, C. E. Anson, A. K. Powell, *Eur. J. Inorg. Chem.* **2005**, 692–703.

[16] Y. Kani, S. Ohba, Yu. Nishida, *Acta Crystallogr., Sect. C* **2000**, *56*, e194.

[17] M. Suzuki, T. Ishikawa, A. Harada, S. Ohba, M. Sakamoto, Y. Nishida, *Polyhedron* **1997**, *16*, 2553–2561.

[18] a) Q. Scheifele, C. Riplinger, F. Neese, H. Weihe, A.-L. Barra, F. Juranyi, A. Podlesnyak, P. L. W. Tregenna-Piggott, *Inorg. Chem.* **2008**, *47*, 439–447; b) H. A. Goodwin, R. S. Sylva, *Aust. J. Chem.* **1967**, *20*, 629–637; c) V. V. Zelentsov, *J. Struct. Chem.* **1967**, *8*, 581.

[19] a) D. Gatteschi, R. Sessoli, J. Villain, *Molecular Nanomagnets*, Oxford University Press, New York, **2006**; b) D. Gatteschi, R. Sessoli, *Angew. Chem. Int. Ed.* **2003**, *42*, 268–297.

[20] a) N. Ishii, Y. Okamura, S. Chiba, T. Nogami, T. Ishida, *J. Am. Chem. Soc.* **2008**, *130*, 24–25; b) T. Ishida, Y. Okamura, I. Watanabe, *Inorg. Chem.* **2009**, *48*, 7012–7014; c) Y. Okamura, T. Nogami, T. Ishida, *Chem. Lett.* **2009**, *38*, 740–741.

[21] a) D. K. Rittenberg, K. Sugiura, Y. Sakata, S. Mikami, A. J. Epstein, J. S. Miller, *Adv. Mater.* **2000**, *12*, 126–130; b) A. J. Epstein, *MRS Bull.* **2000**, *25*, 33–40; c) E. Coronado, C. J. Gómez-García, A. Nuez, F. M. Romero, C. J. Waerenborgh, *Chem. Mater.* **2006**, *18*, 2670–2681; d) S. Vilminot, P. J. Baker, S. J. Blundell, T. Sugano, G. André, M. Kurmoo, *Chem. Mater.* **2010**, *22*, 4090–4095.

[22] a) I. Dzyaloshinskii, *J. Phys. Chem. Solids* **1958**, *4*, 241; b) I. Dzyaloshinskii, *Soviet Phys. JETP* **1958**, *6*, 1120.

[23] a) T. Moriya, *Phys. Rev.* **1960**, *117*, 635–647; b) T. Moriya, *Phys. Rev.* **1960**, *120*, 91–98.

[24] a) X.-Y. Wang, Z.-M. Wang, S. Gao, *Inorg. Chem.* **2008**, *47*, 5720–5726; b) X.-Y. Wang, Z.-M. Wang, S. Gao, *Chem. Commun.* **2008**, 281–294.

[25] a) S. Mossin, H. Weihe, H. O. Sørensen, N. Lima, R. Sessoli, *Dalton Trans.* **2004**, 632–639; b) P. Kar, R. Biswas, M. G. B. Drew, Y. Ida, T. Ishida, A. Ghosh, *Dalton Trans.* DOI: 10.1039/C0DT01521K.

[26] X.-Y. Wang, L. Wang, Z.-M. Wang, S. Gao, *J. Am. Chem. Soc.* **2006**, *128*, 674–675.

[27] a) K. Nakayama, T. Ishida, R. Takayama, D. Hashizume, M. Yasui, F. Iwasaki, T. Nogami, *Chem. Lett.* **1998**, 497–498; b) R. Feyerherm, A. Loose, T. Ishida, T. Nogami, J. Kreitlow, D. Baabe, F. J. Litterst, S. Sullow, H. H. Klauss, K. Doll, *Phys. Rev. B* **2004**, *69*, 134427.

[28] N. Takagami, T. Ishida, T. Nogami, *Bull. Chem. Soc. Jpn.* **2004**, *77*, 1125–1134.

[29] W.-X. Zhang, W. Xue, Y.-Z. Zheng, X.-M. Chen, *Chem. Commun.* **2009**, 3804–3806.

[30] a) S. M. Saadeh, K. L. Trojan, J. W. Kampf, W. E. Hatfield, V. L. Pecoraro, *Inorg. Chem.* **1993**, *32*, 3034–3040; b) K. Mitra, D. Mishra, S. Biswas, C. R. Lucas, B. Adhikary, *Polyhedron* **2006**, *25*, 1681–1688.

[31] a) D. Huang, W. Wang, X. Zhang, C. Chen, F. Chen, Q. Liu, D. Liao, L. Li, L. Sun, *Eur. J. Inorg. Chem.* **2004**, 1454–1464; b) Y. Rodriguez-Martin, M. Hernandez-Molina, J. Sanchiz, C. Ruiz-Perez, F. Lloret, M. Julve, *Dalton Trans.* **2003**, 2359–2365; c) S. Durot, C. Policar, G. Pelosi, F. Bisceglie, T. Mallah, J.-P. Mahy, *Inorg. Chem.* **2003**, *42*, 8072–8080; d) V. Gómez, M. Corbella, *Eur. J. Inorg. Chem.* **2009**, 4471–4482.

[32] a) G. L. Abbati, A. Cornia, A. C. Fabretti, A. Caneschi, D. Gatteschi, *Inorg. Chem.* **1998**, *37*, 1430–1431; b) C. Boskovic, R. Bircher, P. L. W. Tregenna-Piggott, H. U. Güdel, C. Paulsen, W. Wernsdorfer, A. L. Barra, E. Khatsko, A. Neels, H. Stoeckli-Evans, *J. Am. Chem. Soc.* **2003**, *125*, 14046–14058.

[33] a) Y. Feng, J. Xu, D. Liao, S. Yan, Z. Jiang, *J. Coord. Chem.* **2008**, *61*, 3568–3574; b) P. Garge, R. Chikate, S. Padhye, J. M. Savariault, P. De Loth, J.-P. Tuchagues, *Inorg. Chem.* **1990**, *29*, 3315–3320, and references cited therein; c) R. Boca, *Coord. Chem. Rev.* **2004**, *248*, 757–815.

[34] R. Clerac, H. Miyasaka, M. Yamashita, C. Coulon, *J. Am. Chem. Soc.* **2002**, *124*, 12837–12844.

[35] *CrysAlis*, Oxford Diffraction Ltd., Abingdon, U. K., **2006**.

[36] SHELXS97 and SHELXL97, Programs for Crystallographic solution and refinement: G. M. Sheldrick, *Acta Crystallogr., Sect. A* **2008**, *64*, 112–122.

[37] *ABSPACK*, Oxford Diffraction Ltd., Oxford, U. K. **2005**.

Received: November 19, 2010
Published Online: March 29, 2011

